Article

Iodine-Doped 3D Print Ti Alloy for Antibacterial Therapy on Orthopedic Implants

Xiaodong Hu, Jiaqi Zhong, Haiyong Ao, Xinhui Wu, Yujiong Chen, and Zhaoxiang Peng*

Cite This: ACS Omega 2023, 8, 32990−32997

Read Online

ACCESS | lıl Metrics & More | 🔲 Article Recommendations

ABSTRACT: This study presents a novel approach to mitigating bacterial infections and antibiotic resistance in medical implants through the integration of iodine-doping and 3D printing techniques. Iodine, with its potent antibacterial properties, and titanium alloy (Ti), a popular metal for implants due to its mechanical and biological properties, were combined via electrodeposition on 3D-printed titanium alloy (3D-Ti) implants. Scanning electron microscopy, energy dispersive spectroscopy, and X-ray photoelectron spectroscopy confirmed the successful creation of iodine-doped titanium implants with improved iodine content due to the rough surface of the 3D-printed material. In vitro studies revealed that these implants significantly inhibited bacterial adhesion and biofilm formation and showed favorable release kinetics for iodine ions. Biocompatibility tests demonstrated no cytotoxic effects and good hemocompatibility. The implants demonstrated enhanced antimicrobial efficacy against *Escherichia coli* (*E. coli*) and *Staphylococcus aureus* (*S. aureus*) bacteria strains. The findings imply that the integration of iodine-doping and 3D printing technologies is a promising strategy for treating postoperative infections associated with medical implants, consequently bettering the prognosis for patients. Future investigations are encouraged to delve into the long-standing impacts and prospective clinical utility of this groundbreaking methodology.
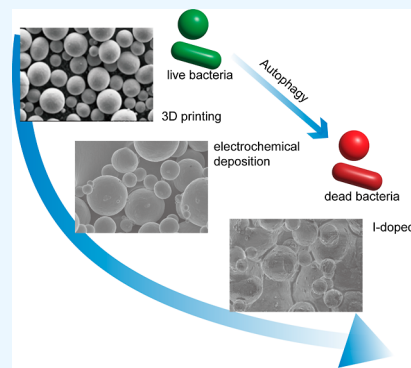
1. INTRODUCTION

With excellent mechanochemical properties, good corrosion resistance, and biocompatibility, titanium and titanium alloys are currently the preferred artificial implant materials in orthopedic surgery.[1,2] However, the surface inertness of titanium metal is prone to poor osseointegration with the host bone after implantation, leading to complications such as loosening or infection, causing serious consequences such as loss of function, surgical failure, or even revision surgery.[3,4] Therefore, the rapid formation of strong and durable osseointegration between the endograft and the host bone is an urgent problem for orthopedic surgeons to solve.

3D printing technology has the great advantage of personalized and precise customization, combining the excellent characteristics of titanium, customizing it according to the patient's original bone structure, creating implants with the same shape and similar microstructure as their bone, using the advantages of shape matching to maximize the recovery of biomechanics, shortening the process of soft tissue readaptation, and better realizing the rapid formation of strong and durable osseointegration between the endophyte and the host bone.[3,5,6]

Despite these advantages of 3D-printed titanium alloys, postorthopedic surgical infections remain a catastrophic complication of orthopedic surgery, causing significant mental and financial damage to patients.[7,8] The main cause of these infections is bacteria adhering and multiplying on the implant surface and forming a biofilm.[9,10] Once bacteria form a biofilm on the implant surface, they resist the immune system's defense and become resistant to the drug.[11−14] To avoid infection, patients have to take high doses of oral or injectable antibiotics for a long time after surgery to prevent infection.[15,16] The antibiotics taken usually work systemically and cause some damage to the body but are not effective enough to act on the surgical site. Therefore, due to the challenges in the treatment of antibiotic-mediated infections, there is an urgent need for antibiotic-free approaches to combat bacterial infections to provide more effective and safer antimicrobial therapy.

In recent years, researchers have designed a range of antimicrobial materials by modifying the surface of titanium-based implants that can impart antimicrobial properties to implants without the use of antibiotics due to their unique properties to specifically interrupt bacterial physiological processes such as DNA replication, cell membrane permeability, etc.[17,18] For example, silver has been incorporated into
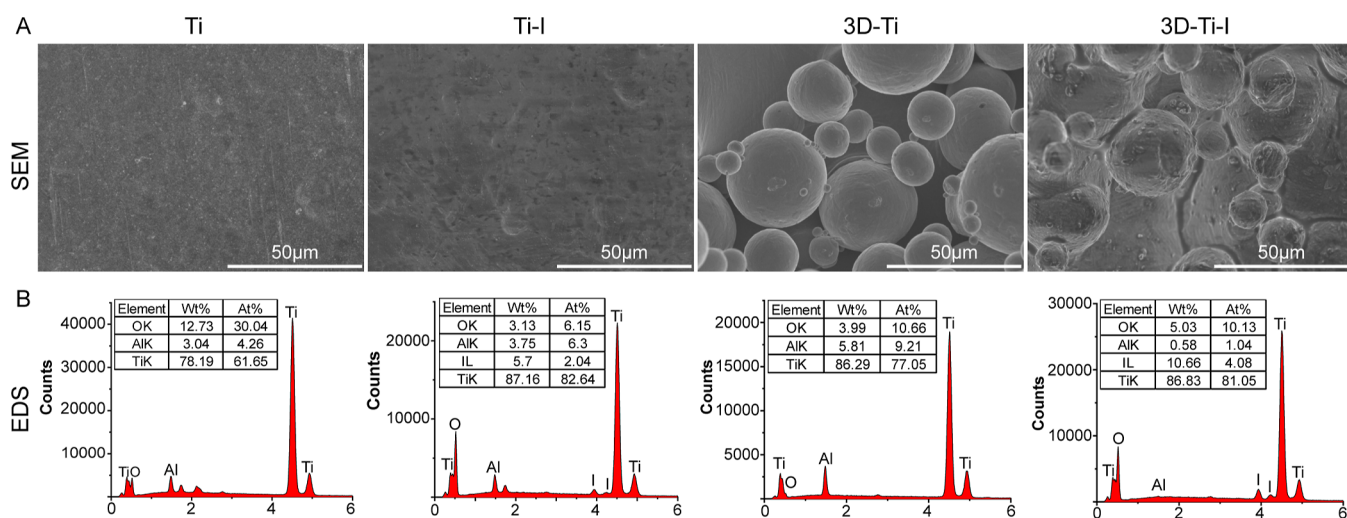
Figure 1. Surface morphology and element content of the implant. (A) Surface morphology of Ti, Ti—I, 3D-Ti, and 3D-Ti—I. (B) EDX pattern of Ti, Ti—I, 3D-Ti, and 3D-Ti—I.
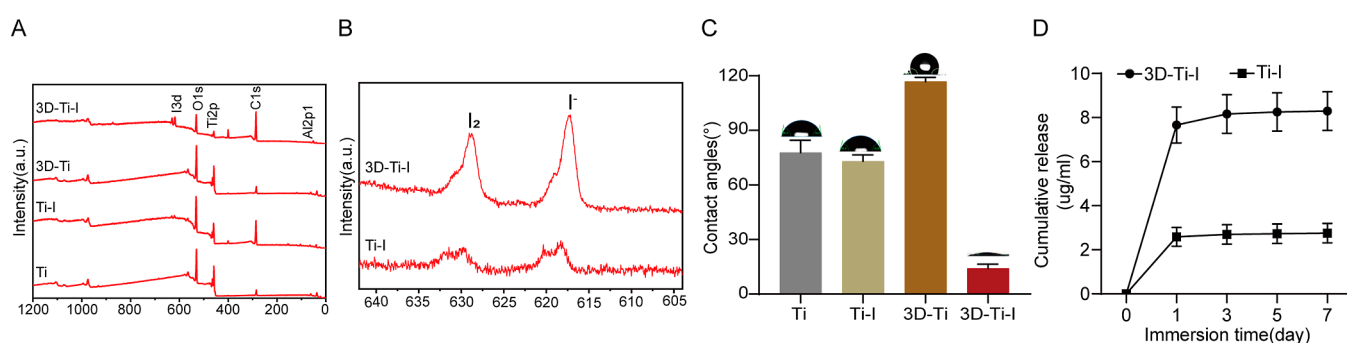
Figure 2. (A) Full peaks of Ti, Ti—I, 3D-Ti, and 3D-Ti—I surface XPS. (B) High-resolution narrow peaks of Ti—I and 3D-Ti—I surface iodine. (C) Water contact angles of Ti, Ti—I, 3D-Ti, and 3D-Ti—I. (D) ICP-MS detection of the cumulative release of Ti—I and 3D-Ti—I from samples in PBS buffer.

a Ti implant surface as silver ions can disrupt bacterial cell membranes and eliminate contact with bacteria.[19,20] Although these strategies have reduced bacterial colonization of implant surfaces and antibiotic misuse, their drawbacks have gradually been identified, which include insufficient drug loading, poor hydrophilicity, and biocompatibility, which in turn limit their clinical application.[19,21,22]

Elemental iodine is an essential trace element that plays an important role in energy metabolism and neurodevelopment in the human body. Thereafter, iodine has strong antibacterial properties, eradicating established biofilms by disrupting the structure of cells and interfering with the expression of genetic material.[23,24] To date, no clinical cases of iodine-induced drug-resistant bacteria have been reported, making iodine an outstanding candidate to replace antibiotics.[25]

Electrodeposition is considered a simple and economical technique for the preparation of surface coatings. A wide range of coating properties (e.g., wettability, corrosion and abrasion resistance, etc.) can be achieved through fine control of deposition parameters such as electrolyte composition, current density, and operating temperature.[26,27]

Aiming at these problems, in this study we combined 3D printing technology with electrochemical deposition to address insufficient drug loading, poor hydrophilicity, and biocompatibility faced by orthopedic implants. We utilized 3D printing technology to improve surface bone integration and drug loading and electrochemical deposition to alter the surface wettability and form a consistent, even layer of iodine on a 3D-printed titanium implant. We performed in vitro studies to demonstrate the effectiveness of iodine-doped titanium implants in inhibiting bacterial adhesion and biofilm formation, which are critical factors in the development of implant-associated infections. Furthermore, the potential for controlled and sustained release of iodine from the implant surface offers a promising strategy for maintaining long-term antibacterial activity without negatively affecting the surrounding tissue.

2. MATERIALS AND METHODS

Unless specified, chemicals were purchased from Shanghai Aladdin Biochemical Technology Co., Ltd.

2.1. Fabrication of 3D-Printed Titanium Implant. Ti—6Al—4 V powder and sheets used in this experiment were prepared by the Ningbo Branch of the Chinese Academy of Weapons Science. The Ti—6Al—4 V powder was synthesized by using the electrode induction gas atomization (EIGA) method. The powder was spherical or nearly spherical (sphericity = 0.9, typical particle size range is 15—53 μm). The additive manufacturing process was conducted with an EOS M290. The parameters for the printing process are listed as follows, P = 280 W, h = 0.03 mm, d = 0.14 mm, and v = 1200 mm/s, in which P represents the laser power (W), h represents the layer thickness of the layered powder (mm), d
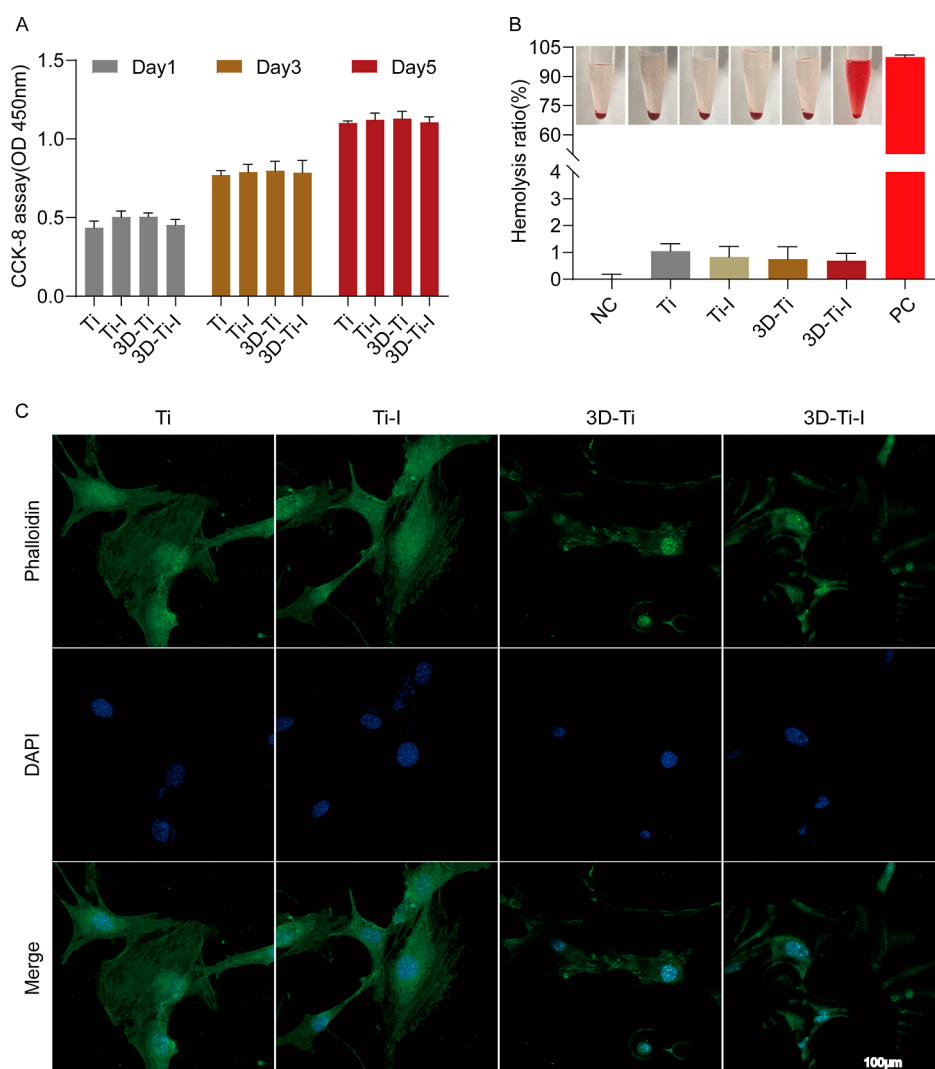
Figure 3. Biocompatibility of implants. (A) MC3T3-E1 cell viability was evaluated with cck-8. (B) Hemolysis assay. (C) MC3T3-E1 cell adhesion, stained with FITC-phalloidin and DAPI.

represents the line spacing (mm), and v represents the laser scanning speed (mm/s); hence, the energy density of the process could be described as formula 1

$$E = \frac{P}{h \cdot v \cdot d} \tag{1}$$

2.2. Doping of Iodine. After cleaning with acetone and alcohol, titanium alloy samples were placed at the anode of an electrophoresis tank; the cathode was a stainless steel plate, and the cathode and anode plates were spaced 10 cm apart. A mixture of 0.4 wt % polyvinylpyrrolidone iodine and 0.4 wt % KI solution was used as the electrolyte. The reaction was then carried out under a constant voltage of 15 V for 30 min with protection from light. After the reaction, the surface of the sample was rinsed three times with deionized water to remove unbound impurities and then dried with cold air for subsequent experiments.

2.3. Characterization of Implants. Scanning electron microscopy (SEM) (Hitachi SU-70, Japan) and energy dispersive spectroscopy (EDS) were performed to observe surface topography and determine the elemental content of implants. X-ray photoelectron spectroscopy (XPS) was used to determine the surface element content and the chemical state

of the laden element. Water contact angle measurements were conducted by using a contact angle instrument (KRUSS DSA25S, China). Ti and 3D-Ti cylinders with a diameter of 5 mm and a height of 2 mm were tested for mechanical properties using a universal testing machine (Instron, USA). The porosity was detected by a Micro-CT (PINGSENG Healthcare Inc., China). The release profile was assessed by submerging the implants in PBS at 37 °C. The iodine content was determined with ICP-MS (Agilent 7800, USA).

2.4. In Vitro Biocompatibility Assay. MC3T3-E1 subclone 14 (CAS, China) cells were cultured in 10% FBS (Corning, USA) supplemented MEM-α (Vivacell, China) under 5% CO_2 and 37 °C. Cellular compatibility assays were performed by directly culturing cells on the implant. A total of $5 \times 1 \times 10^3$ cells were seeded onto the implant in a 96-well plate. On days 1, 3, and 5, the cck-8 assay was performed according to the manufacturer's protocol. Cell adhesion was observed with confocal laser scanning microscopy (CLSM, Leica SP8, Germany). After 1 day of culturing, attached cells were fixed in paraformaldehyde permeabilized with 0.2% Triton X-100 and stained with phalloidin-FITC and DAPI.

For the hemolytic assay, Triton X-100 (1%) and saline (0.9%) were employed as positive control (PC) and negative
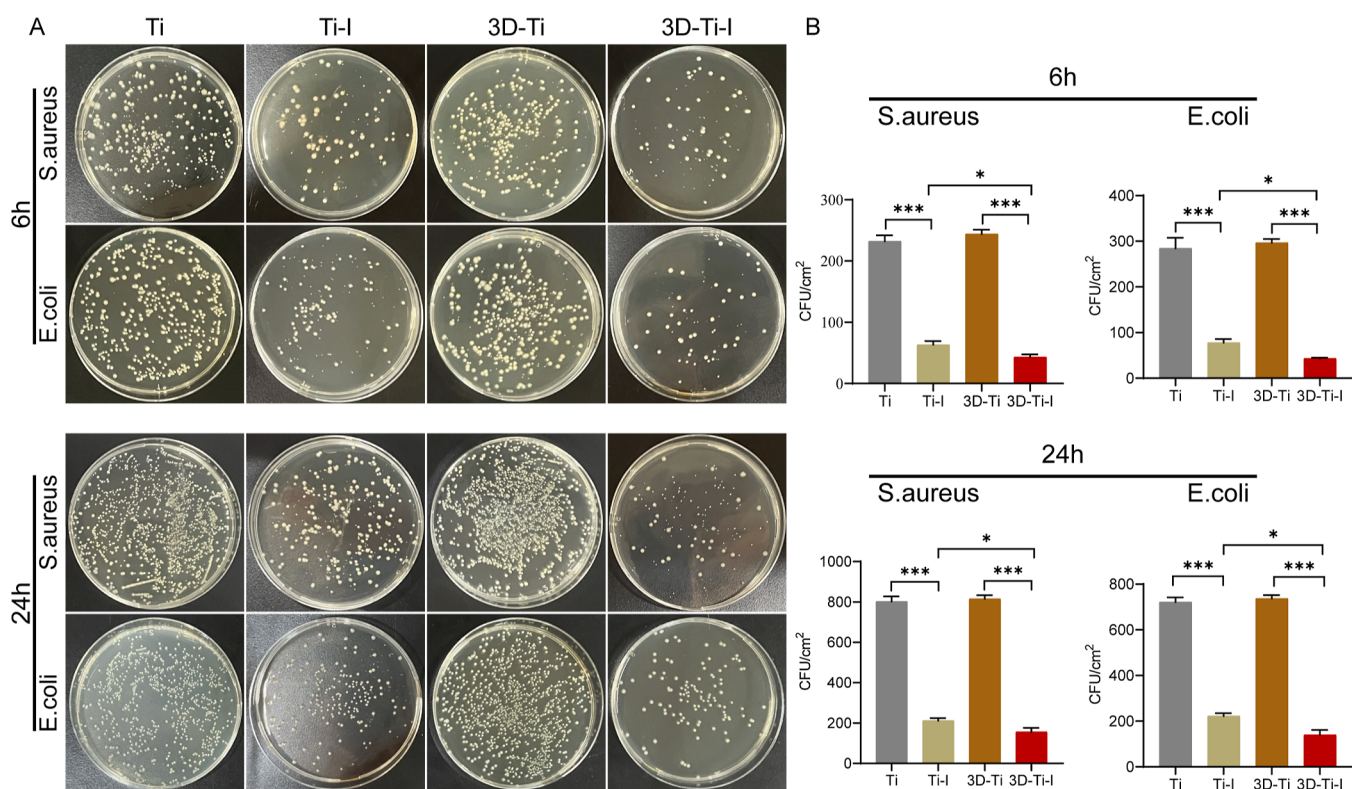
Figure 4. (A) Plate colony counts result from the antibacterial effect of the iodine-doped implant. (B) Quantified outcomes of the plate count.

control (NC) samples and were added to the centrifuge tubes, respectively. Then, equal amount of RBC saline resuspension was added to each tube. The centrifuge tubes were then incubated in a 37 °C incubator for 3 h. Finally, all tubes were centrifuged at 1600 rpm for 8 min, and the absorbance of the supernatant was measured at 545 nm. The hemolysis rate was calculated according to formula 2

$$\text{hemolysis rate (\%)} = \frac{(A_s - A_{nc})}{(A_{pc} - A_{nc})} \times 100\% \tag{2}$$

where A_s, A_{nc}, and A_{pc} are the absorbance values of the experimental group, negative control group, and positive control group, respectively.

2.5. Antibacterial Effect of Iodine-Doped Implant. The antibacterial effect of the samples was evaluated with the plate counting method. The samples were UV sterilized and placed in a 24-well plate. After rinsing three times with PBS, 1 mL of 1.0×10^6 cfu/mL tryptic soy broth (TSB) *Staphylococcus aureus* (*S. aureus*) or *Escherichia coli* (*E. coli*) suspension was added to each well. After incubating statically for 24 h at 37 °C, the samples were sonicated for 5 min to disassociate the adhered bacteria. The sonicated bacteria suspension was inoculated to PCA agar plates and incubated for 24 h before counting bacterial colonies.

The antibacterial properties of the samples were determined by live−dead fluorometry. After 24 h of coincubation with TSB bacterial suspension, the samples were washed three times with PBS and tested for bacterial viability using the LIVE/DEAD BacLight Bacterial Viability Kit (L7012, Thermos Fisher Scientific, USA) according to the manufacturer's protocol. Samples were observed using CLSM.

2.6. Reactive Oxygen Species Levels. Intracellular levels of reactive oxygen species (ROS) were measured with the

fluorescent probe 2′,7′-dichlorodihydrofluorescein diacetate (DCFH-DA, Beyotime, Shanghai, China). DCFH-DA can be deacetylated and oxidized after crossing the membrane of living bacteria to form fluorescent 2′,7′-dichlorofluorescein (DCF). The fluorescence intensity of DCF was detected by CLSM. Bacteria grown on cell plates without any intervention were used as negative controls (NCs). Samples were incubated with bacterial suspensions under 37 °C for 24 h before the original medium was removed, and the samples were rinsed three times with PBS. The samples were then stained with DCFH-DA for 30 min under dark conditions, followed by the removal of excess dye by PBS. Finally, the samples were observed by CLSM.

3. RESULTS AND DISCUSSION

3.1. Fabrication and Characterization of Implant. As illustrated in Figure 1, SEM and EDS were employed to examine the surface morphology and elemental composition. The morphologies of Ti and 3D-Ti differ significantly. The titanium alloy exhibits a smooth surface, whereas 3D-Ti displays micrometer-sized spherical structures resulting from the additive manufacturing process. Upon loading iodine onto the substrate, a noticeable morphological change was observed, as evidenced by comparing iodine-doped 3D-printed Ti alloy (3D-Ti−I) with 3D-Ti. The successful incorporation of iodine was further corroborated by EDS, showing 10.66 wt % iodine content in 3D-Ti−I and 5.7 wt % in iodine-doped Ti alloy (Ti−I). There is no evident change in mechanical properties between 3D-Ti and Ti as the porosity of 3D-Ti is ∼8.3%. The enhancement in loading content may be attributed to the rough surface of 3D-Ti, which facilitates iodine attachment and adherence to the substrate, thus enhancing the loading efficiency.
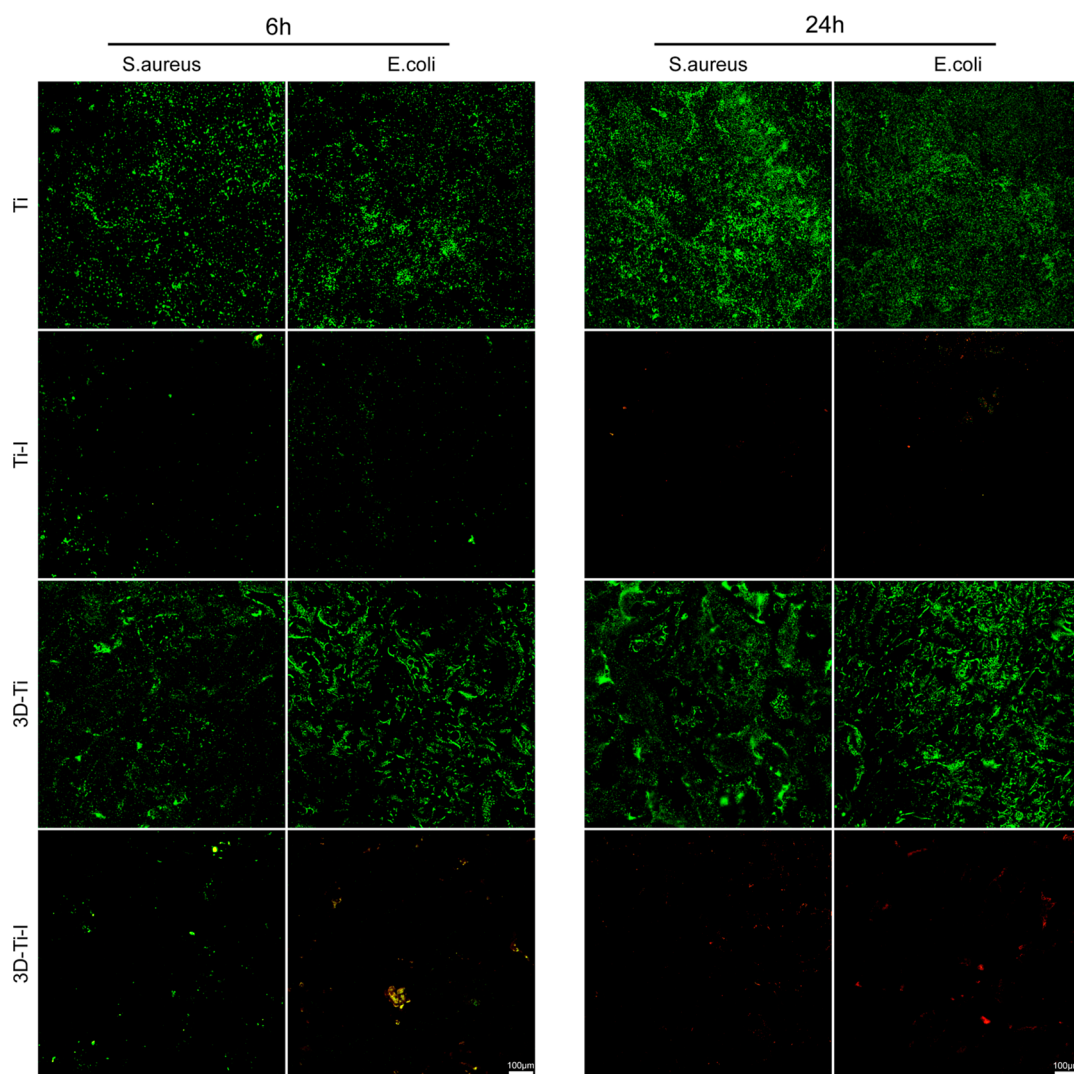
Figure 5. Live/Dead staining of *S. aureus* and *E. coli* on the surfaces of implants.

As shown in Figure 2, we investigated the superficial element's chemical state with XPS, and the laden iodine is observed to be a mixture of iodine monomers with I^-. The iodine monomer and I^- peaks are at ~630.0 and 617.35 eV (Figure 2B). Figure 2C depicts that the surface of Ti−I (73.03° ± 3.48°) and 3D-Ti−I (14.17° ± 2.26°) sheets become more hydrophilic compared with those of Ti (77.70° ± 6.88°) and 3D-Ti (116.9° ± 2.21°). The release profile of iodide ions in the Ti−I and 3D-Ti−I groups for 7 days is shown in Figure 2D. An initial burst release of iodide ions was observed on the first day; this indicates the rapid release of iodine ions from the Ti−I and 3D-Ti−I surfaces, followed by an equilibrium release on days 3, 5, and 7. Whereas the initial adhesion time of the bacteria on the surface of the implant is 4−6 h, and once stable bacterial adhesion is formed, the biofilm is formed within 12−18 h. The explosive release of iodine thus ensures that the bacteria are eliminated or suppressed at an early stage. In addition, the 3D-Ti−I group released more iodide ions than did the Ti−I group, matching the results of Figure 2A,B.

3.2. Biocompatibility of Iodine-Doped Implant. The biocompatibility of medical implants is crucial for their successful application. In this study, we evaluated cytotoxicity, hemocompatibility, and cell adhesion. MC3T3-E1 preosteo-blasts were used to assess cytotoxicity and cell adhesion. As depicted in Figure 3A, no cytotoxicity was observed during the 5 day culturing period, indicating that neither 3D printing nor iodine doping adversely affected cell growth on the implant. This result is further supported by the cell adhesion assay shown in Figure 3C. Adhered cells were stained with FITC-phalloidin and DAPI. No significant differences were observed between the iodine-laden group and the substrate.

Numerous studies have demonstrated the beneficial effects of rough surfaces on bone regeneration and cell adhesion, suggesting that the granulated structure could be advantageous in an in vivo environment.[28,29] This structure may lead to increased pull-out force and improved tissue regeneration.[30] In addition to these findings, we assessed hemocompatibility to ensure the implant's compatibility with blood components and prevent thrombus formation, a critical factor in the perform-ance of medical implants.[31] As shown in Figure 3B, the results indicated no significant adverse effects on blood compatibility, further supporting the implant's biocompatibility.

Despite these promising results, further investigation is still required to determine the precise influence of the granulated structure on the physiological response. Future studies should focus on the long-term effects of the granulated structure on cell behavior, tissue integration, and overall implant perform-
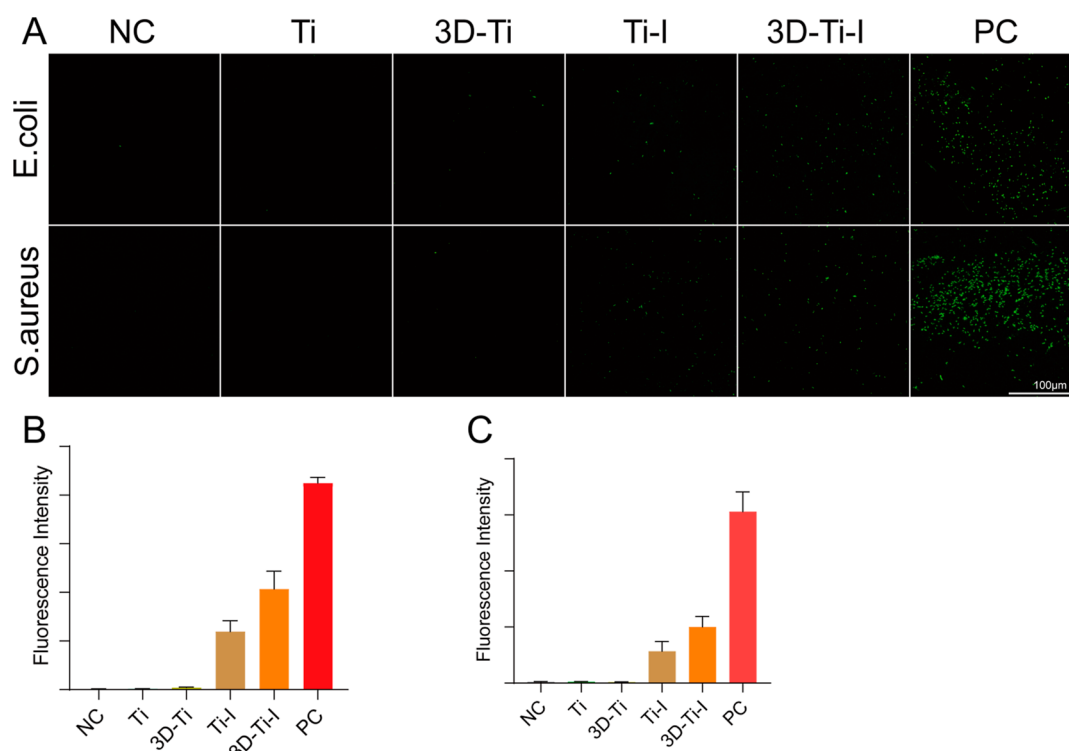
Figure 6. Antibacterial mechanism for the Ti−I and 3D-Ti−I groups. (A) Intracellular ROS fluorescent signal of the bacteria on the different substrates (green fluorescent signal shows the DCF). (B) Quantitative analysis and (C) ROS intensity of *E. coli* and *S. aureus*.

ance. By expanding our understanding of these factors, we can optimize the implant design and fabrication process, ultimately enhancing the success rate of medical implants in various clinical applications.

3.3. Antibacterial Effect of Iodine-Doped Implant. A large body of literature indicates that bacterial infection is one of the main causes of the clinical failure of titanium and titanium alloys as orthopedic implants.[32,33] Once bacterial adhesion occurs on the implant surface, bacterial colonies and biofilms will gradually form and disrupt the function of the implant.[34,35] Previous studies have shown that the early 4−6 h of bacterial adhesion is essential for long-term resistance to bacterial-associated infections and is particularly important.[36,37]

To reveal the antimicrobial properties of different titanium surfaces, the antimicrobial effect of the titanium surfaces was measured by the plate counting method after 6 and 24 h of cocultivation of bacteria with the materials, respectively, *S. aureus* and *E. coli,* which were tested for their in vitro antibacterial activity. As illustrated in Figure 4, both Gram-positive and Gram-negative bacteria exhibited significantly reduced growth when treated with iodine-doped implants. Additionally, we observed that the antibacterial activity of 3D-printed titanium implants with iodine (3D-Ti−I) was significantly more effective than that of conventional titanium implants with iodine (Ti−I).

This enhanced antibacterial effect could be attributed to the increased surface area of 3D-Ti, which allows for a greater amount of iodine to be loaded onto the implant. Moreover, the rough and granulated surface of 3D-Ti may facilitate better contact between the iodine-doped implant and the bacteria, increasing the efficacy of the antibacterial action. This finding underscores the potential of 3D-printed implants with iodine

for combating a broader spectrum of bacterial infections and reducing the risk of implant-associated infections.

By understanding the role of surface properties, such as porosity and wettability, in the bactericidal action of iodine-doped 3D-printed titanium implants, as well as the release kinetics of iodine from the implant surface and its interaction with bacterial cells, we can develop more effective strategies for optimizing the antibacterial properties of medical implants. This will ultimately contribute to reducing the risk of postoperative infections and improving patient outcomes.

To gain additional insights into the antimicrobial effect of the fabricated implants, we conducted live/dead staining of *E. coli* and *S. aureus* on the surfaces of the implants. As demonstrated in Figure 5, the bacteria on 3D-Ti appeared to be localized in the indentations of the 3D-Ti structure. This unique distribution pattern could hinder biofilm formation, further contributing to the antimicrobial properties of the implant.

The antimicrobial effect of iodine-doped implants is evident on the implant surface. The number of bacteria is significantly reduced, with only a few dead bacteria detected as red in the image. This observation suggests that the iodine-doped implants not only inhibit bacterial growth but also actively induce bacterial cell death, thereby enhancing the overall antimicrobial activity. The combination of 3D-Ti's structural features and iodine doping appears to provide a synergistic effect, leading to an even more potent antimicrobial response. The rough and granulated surface of the 3D-Ti implant, coupled with the presence of iodine, creates a hostile environment for bacterial colonization and biofilm development.

3.4. Antibacterial Mechanism of the Iodine-Doped Implant. We conducted a preliminary study of the antibacterial mechanism of iodine-doped implants. Numerous

previous studies have shown that intracellular ROS production is a key mechanism for the effective killing of invading bacteria.[24,38−40] In this study, the fluorescence intensity of DCF was used to respond to the intracellular ROS level of bacteria. As shown in Figure 6A, significant green fluorescence signal was observed in the 3D-Ti−I group compared with the control group. These results suggest that 3D-Ti−I can induce the production of intracellular ROS in bacteria. Quantitative analysis of ROS staining showed that iodine doping on the 3D-Ti significantly increased intracellular ROS in bacteria attached to the surfaces (Figure 6B,C).

4. CONCLUSIONS

In this study, we fabricated an iodine-doped 3D-printed Ti alloy for antibacterial therapy on orthopedic implants. Compared with the iodine-doped titanium alloy, the results showed that the iodine-doped 3D-printed titanium alloy is loaded with more iodine and has better hydrophilicity as well as a better antibacterial effect and no obvious cellular toxicity. Therefore, this material is a promising candidate for the treatment of implant-associated infections.

■ ASSOCIATED CONTENT

Data Availability Statement

All relevant data are within the paper.

■ AUTHOR INFORMATION

Corresponding Author

　Zhaoxiang Peng − *The Affiliated Lihuili Hospital, Ningbo University, Ningbo 315040, China;* orcid.org/0000-0001-6508-4100; Phone: +86 574 8701 8511; Email: pzxao@hotmail.com; Fax: +86 574 8701 8701

Authors

　Xiaodong Hu − *The Affiliated Lihuili Hospital, Ningbo University, Ningbo 315040, China*

　Jiaqi Zhong − *The Affiliated Lihuili Hospital, Ningbo University, Ningbo 315040, China*

　Haiyong Ao − *Jiangxi Key Laboratory of Nanobiomaterials & School of Materials Science and Engineering, East China Jiaotong University, Nanchang 330000, China;* orcid.org/0000-0002-7967-2648

　Xinhui Wu − *Xianju County People's Hospital, Taizhou 317300, China*

　Yujiong Chen − *The Affiliated Lihuili Hospital, Ningbo University, Ningbo 315040, China*

Complete contact information is available at:
https://pubs.acs.org/10.1021/acsomega.3c04721

Notes

The authors declare no competing financial interest.

■ ACKNOWLEDGMENTS

■ REFERENCES

(1) Koons, G. L.; Diba, M.; Mikos, A. G. Materials Design for Bone-Tissue Engineering. *Nat. Rev. Mater.* **2020**, 5 (8), 584−603.

(2) Shah, F. A.; Thomsen, P.; Palmquist, A. Osseointegration and Current Interpretations of the Bone-Implant Interface. *Acta Biomater.* **2019**, 84, 1−15.

(3) Cai, X.; Cai, J.; Ma, K.; Huang, P.; Gong, L.; Huang, D.; Jiang, T.; Wang, Y. Fabrication and Characterization of Mg-Doped Chitosan-Gelatin Nanocompound Coatings for Titanium Surface Functionalization. *J. Biomater. Sci., Polym. Ed.* **2016**, 27 (10), 954−971.

(4) Ren, N.; Li, J.; Qiu, J.; Sang, Y.; Jiang, H.; Boughton, R. I.; Huang, L.; Huang, W.; Liu, H. Nanostructured Titanate with Different Metal Ions on the Surface of Metallic Titanium: A Facile Approach for Regulation of RBMSCs Fate on Titanium Implants. *Small* **2014**, 10 (15), 3169−3180.

(5) Pan, S.; Yin, J.; Yu, L.; Zhang, C.; Zhu, Y.; Gao, Y.; Chen, Y. 2D MXene-Integrated 3D-Printing Scaffolds for Augmented Osteosarcoma Phototherapy and Accelerated Tissue Reconstruction. *Advanced Science* **2020**, 7 (2), 1901511.

(6) Nune, K. C.; Kumar, A.; Murr, L. E.; Misra, R. D. K. Interplay between Self-Assembled Structure of Bone Morphogenetic Protein-2 (BMP-2) and Osteoblast Functions in Three-Dimensional Titanium Alloy Scaffolds: Stimulation of Osteogenic Activity. *J. Biomed. Mater. Res., Part A* **2016**, 104 (2), 517−532.

(7) Ferguson, R. J.; Palmer, A. J.; Taylor, A.; Porter, M. L.; Malchau, H.; Glyn-Jones, S. Hip Replacement. *Lancet* **2018**, 392 (10158), 1662−1671.

(8) Morgenstern, M.; Kühl, R.; Eckardt, H.; Acklin, Y.; Stanic, B.; Garcia, M.; Baumhoer, D.; Metsemakers, W.-J. Diagnostic Challenges and Future Perspectives in Fracture-Related Infection. *Injury* **2018**, 49, S83−S90.

(9) Zhu, X.; Zhang, K.; Lu, K.; Shi, T.; Shen, S.; Chen, X.; Dong, J.; Gong, W.; Bao, Z.; Shi, Y.; Ma, Y.; Teng, H.; Jiang, Q. Inhibition of Pyroptosis Attenuates Staphylococcus Aureus-Induced Bone Injury in Traumatic Osteomyelitis. *Ann. Transl. Med.* **2019**, 7 (8), 170.

(10) Urish, K. L.; Cassat, J. E. Staphylococcus Aureus Osteomyelitis: Bone, Bugs, and Surgery. *Infect. Immun.* **2020**, 88(7), e00932−e00919..

(11) Tzeng, A.; Tzeng, T. H.; Vasdev, S.; Korth, K.; Healey, T.; Parvizi, J.; Saleh, K. J. Treating Periprosthetic Joint Infections as Biofilms: Key Diagnosis and Management Strategies. *Diagn. Microbiol. Infect. Dis.* **2015**, 81 (3), 192−200.

(12) Singh, S.; Datta, S.; Narayanan, K. B.; Rajnish, K. N. Bacterial Exo-Polysaccharides in Biofilms: Role in Antimicrobial Resistance and Treatments. *J. Genet. Eng. Biotechnol.* **2021**, 19 (1), 140.

(13) Amin Yavari, S.; Castenmiller, S. M.; Strijp, J. A. G.; Croes, M. Combating Implant Infections: Shifting Focus from Bacteria to Host. *Adv. Mater.* **2020**, 32 (43), 2002962.

(14) Sahoo, J.; Sarkhel, S.; Mukherjee, N.; Jaiswal, A. Nanomaterial-Based Antimicrobial Coating for Biomedical Implants: New Age Solution for Biofilm-Associated Infections. *ACS Omega* **2022**, 7 (50), 45962−45980.

(15) Turner, N. A.; Sharma-Kuinkel, B. K.; Maskarinec, S. A.; Eichenberger, E. M.; Shah, P. P.; Carugati, M.; Holland, T. L.; Fowler, V. G. Methicillin-Resistant Staphylococcus Aureus: An Overview of Basic and Clinical Research. *Nat. Rev. Microbiol.* **2019**, 17 (4), 203−218.

(16) Anderson, P. A.; Savage, J. W.; Vaccaro, A. R.; Radcliff, K.; Arnold, P. M.; Lawrence, B. D.; Shamji, M. F. Prevention of Surgical Site Infection in Spine Surgery. *Neurosurgery* **2017**, 80 (3S), S114−S123.

(17) Oduwole, K. O.; Glynn, A. A.; Molony, D. C.; Murray, D.; Rowe, S.; Holland, L. M.; McCormack, D. J.; O'Gara, J. P. Anti-Biofilm Activity of Sub-Inhibitory Povidone-Iodine Concentrations against Staphylococcus Epidermidis and Staphylococcus Aureus. *J. Orthop. Res.* **2010**, 28 (9), 1252−1256.

(18) Hoekstra, M. J.; Westgate, S. J.; Mueller, S. Povidone-Iodine Ointment Demonstrates in Vitro Efficacy against Biofilm Formation. *Int. Wound J.* **2017**, *14* (1), 172−179.

(19) Jin, J.; Fei, D.; Zhang, Y.; Wang, Q. Functionalized titanium implant in regulating bacteria and cell response. *Int. J. Nanomed.* **2019**, *14*, 1433−1450.

(20) Peng, C.; Zhao, Y.; Jin, S.; Wang, J.; Liu, R.; Liu, H.; Shi, W.; Kolawole, S. K.; Ren, L.; Yu, B.; Yang, K. Antibacterial TiCu/TiCuN Multilayer Films with Good Corrosion Resistance Deposited by Axial Magnetic Field-Enhanced Arc Ion Plating. *ACS Appl. Mater. Interfaces* **2019**, *11* (1), 125−136.

(21) Yallapu, M. M.; Nagesh, P. K. B.; Jaggi, M.; Chauhan, S. C. Therapeutic Applications of Curcumin Nanoformulations. *AAPS J.* **2015**, *17* (6), 1341−1356.

(22) Mahmood, K.; Zia, K. M.; Zuber, M.; Salman, M.; Anjum, M. N. Recent Developments in Curcumin and Curcumin Based Polymeric Materials for Biomedical Applications: A Review. *Int. J. Biol. Macromol.* **2015**, *81*, 877−890.

(23) Kozlovska, I. M.; Romanjuk, N. Y.; Romanjuk, L. M.; Kukhtyn, M. D.; Horiuk, Y. V.; Karpyk, G. V. The Effect of Antimicrobial Agents on Planktonic and Biofilm Forms of Bacteria That Are Isolated from Chronic Anal Fissures. *Regul. Mech. Biosyst.* **2017**, *8* (4), 577−582.

(24) Teng, W.; Zhang, Z.; Wang, Y.; Ye, Y.; Yinwang, E.; Liu, A.; Zhou, X.; Xu, J.; Zhou, C.; Sun, H.; Wang, F.; Zhang, L.; Cheng, C.; Lin, P.; Wu, Y.; Gou, Z.; Yu, X.; Ye, Z. Iodine Immobilized Metal-Organic Framework for NIR-Triggered Antibacterial Therapy on Orthopedic Implants. *Small* **2021**, *17* (35), 2102315.

(25) Bigliardi, P. L.; Alsagoff, S. A. L.; El-Kafrawi, H. Y.; Pyon, J.-K.; Wa, C. T. C.; Villa, M. A. Povidone Iodine in Wound Healing: A Review of Current Concepts and Practices. *Int. J. Oral Surg.* **2017**, *44*, 260−268.

(26) Yue, B.; Zhu, G.; Chang, Z.; Song, J.; Gao, X.; Wang, Y.; Guo, N.; Zhai, X. Study on Surface Wettability of Nickel Coating Prepared by Electrodeposition Combined with Chemical Etching. *Surf. Coat. Technol.* **2022**, *444*, 128695.

(27) Torabinejad, V.; Aliofkhazraei, M.; Assareh, S.; Allahyarzadeh, M. H.; Rouhaghdam, A. S. Electrodeposition of Ni-Fe Alloys, Composites, and Nano Coatings-A Review. *J. Alloys Compd.* **2017**, *691*, 841−859.

(28) Metwally, S.; Ferraris, S.; Spriano, S.; Krysiak, Z. J.; Kaniuk, Ł.; Marzec, M. M.; Kim, S. K.; Szewczyk, P. K.; Gruszczyński, A.; Wytrwal-Sarna, M.; Karbowniczek, J. E.; Bernasik, A.; Kar-Narayan, S.; Stachewicz, U. Surface Potential and Roughness Controlled Cell Adhesion and Collagen Formation in Electrospun PCL Fibers for Bone Regeneration. *Mater. Des.* **2020**, *194*, 108915.

(29) Wang, M.; Favi, P.; Cheng, X.; Golshan, N. H.; Ziemer, K. S.; Keidar, M.; Webster, T. J. Cold Atmospheric Plasma (CAP) Surface Nanomodified 3D Printed Polylactic Acid (PLA) Scaffolds for Bone Regeneration. *Acta Biomater.* **2016**, *46*, 256−265.

(30) Kelly, C. N.; Miller, A. T.; Hollister, S. J.; Guldberg, R. E.; Gall, K. Design and Structure-Function Characterization of 3D Printed Synthetic Porous Biomaterials for Tissue Engineering. *Adv. Healthcare Mater.* **2018**, *7* (7), 1701095.

(31) Badv, M.; Bayat, F.; Weitz, J. I.; Didar, T. F. Single and Multi-Functional Coating Strategies for Enhancing the Biocompatibility and Tissue Integration of Blood-Contacting Medical Implants. *Biomaterials* **2020**, *258*, 120291.

(32) Chouirfa, H.; Bouloussa, H.; Migonney, V.; Falentin-Daudré, C. Review of Titanium Surface Modification Techniques and Coatings for Antibacterial Applications. *Acta Biomater.* **2019**, *83*, 37−54.

(33) Yang, F.; Zhang, Z.; Li, Y.; Xiao, C.; Zhang, H.; Li, W.; Zhan, L.; Liang, G.; Chang, Y.; Ning, C.; Zhai, J.; Zhou, Z.; Yu, P. In Situ Construction of Black Titanium Oxide with a Multilevel Structure on a Titanium Alloy for Photothermal Antibacterial Therapy. *ACS Biomater. Sci. Eng.* **2022**, *8* (6), 2419−2427.

(34) Wu, S.; Xu, J.; Zou, L.; Luo, S.; Yao, R.; Zheng, B.; Liang, G.; Wu, D.; Li, Y. Long-Lasting Renewable Antibacterial Porous Polymeric Coatings Enable Titanium Biomaterials to Prevent and Treat Peri-Implant Infection. *Nat. Commun.* **2021**, *12* (1), 3303.

(35) Chen, X.; Zhou, J.; Qian, Y.; Zhao, L. Antibacterial Coatings on Orthopedic Implants. *Mater. Today Bio* **2023**, *19*, 100586.

(36) Campoccia, D.; Montanaro, L.; Arciola, C. R. A Review of the Biomaterials Technologies for Infection-Resistant Surfaces. *Biomaterials* **2013**, *34* (34), 8533−8554.

(37) Xu, G.; Shen, X.; Dai, L.; Ran, Q.; Ma, P.; Cai, K. Reduced Bacteria Adhesion on Octenidine Loaded Mesoporous Silica Nanoparticles Coating on Titanium Substrates. *Mater. Sci. Eng. C* **2017**, *70*, 386−395.

(38) Precious Ayanwale, A.; Reyes-López, S. Y. ZrO2-ZnO Nanoparticles as Antibacterial Agents. *ACS Omega* **2019**, *4* (21), 19216−19224.

(39) Shivalkar, S.; Arshad, F.; Sahoo, A. K.; Sk, M. P. Visible Light-Mediated Photoactivated Sulfur Quantum Dots as Heightened Antibacterial Agents. *ACS Omega* **2022**, *7* (37), 33358−33364.

(40) Nie, X.; Wu, S.; Huang, F.; Wang, Q.; Wei, Q. Smart Textiles with Self-Disinfection and Photothermochromic Effects. *ACS Appl. Mater. Interfaces* **2021**, *13* (2), 2245−2255.